

MEASUREMENTS USING A POLARIZATION INSTRUMENTATION RADAR ON SELECTED TARGETS

I.D. Olin and F.D. Queen

**Tracking Branch
Radar Division**

April 18, 1962



**U. S. NAVAL RESEARCH LABORATORY
Washington, D.C.**

**APPROVED FOR PUBLIC
RELEASE - DISTRIBUTION
UNLIMITED**

**MEASUREMENTS USING A
POLARIZATION INSTRUMENTATION
RADAR ON SELECTED TARGETS**

**MEASUREMENTS USING A POLARIZATION
INSTRUMENTATION RADAR ON SHIPS,
AIRCRAFT, SEA RETURN, AND CHAFF**

I.D. Olin and F.D. Queen

Tracking Branch
Radar Division

April 18, 1962



**U. S. NAVAL RESEARCH LABORATORY
Washington, D.C.**

This page intentionally left blank.

CONTENTS

Abstract	ii
Problem Status	ii
Authorization	ii
INTRODUCTION	1
RADAR AND DATA-RECORDING SYSTEM	1
EXPERIMENTAL DATA	2
Ships and Aircraft	2
Sea Return, Chaff, and Operational Aircraft	3
AUTOCORRELATION AND CROSSCORRELATION FUNCTIONS	5
CORRELATION FUNCTIONS OF POLARIZED COMPONENTS	5
INTERPRETATION OF COMPUTED RESULTS	7
CONCLUSIONS	7
ACKNOWLEDGMENTS	7
REFERENCES	8

ABSTRACT

An X-band pulsed radar system designed to measure echoing area and target-polarization characteristics has been built. Transmission of any one of four polarized components is possible (vertical, horizontal, right circular, and left circular), and the system is capable of receiving simultaneously along all four resolved components.

Tests have been conducted on a variety of ships, and polarized component return has been calibrated and recorded for different transmitted polarizations. Tests on propeller-driven aircraft (Convair 240 and a T-28) indicate the behavior of such factors as propeller modulation on polarized component return. An F3H jet aircraft was examined during flight and while dispensing chaff. Echo-area calibration indicates nose-on and broadside cross-section areas on the order of 120 and 12,000 sq ft, respectively.

The characteristics of chaff and sea return have been examined in detail. The properties of the crosscorrelation of orthogonally polarized returns have been considered and applied to these two targets. Large positive values of crosscorrelation are associated with gross area changes, whereas polarization changes are associated with large negative values of crosscorrelation. Although the return from chaff and the sea appears equally noisy, sea return displays prominent power fading, whereas the chaff also displays polarization changes.

PROBLEM STATUS

This is an interim report on one phase of the problem; work on this and other phases is continuing.

AUTHORIZATION

NRL Problem R07-04
Project RR 008-01-41-5552

Manuscript submitted January 25, 1962.

MEASUREMENTS USING A POLARIZATION INSTRUMENTATION RADAR ON SELECTED TARGETS

INTRODUCTION (UNCLASSIFIED)

This report describes results of the final tests using the interim polarization radar described in a previous NRL report. The purpose of these tests was to examine several different target types and to evaluate the suitability of this system for the measurement of the radar echoing area and polarization characteristics. The earlier work described the system details and performance limitations. In addition, a series of tests on radar navigational buoys was conducted and reported. Particular note was made of the radar performance of the buoys on circular polarization. These buoys had been designed previously for use with linear polarization alone.

The targets used in the tests described here were all "targets of opportunity," so precise description is not always possible. Since the system details and performance limitations have already been discussed in the first report, much of this is not presented here.

RADAR AND DATA-RECORDING SYSTEM (UNCLASSIFIED)

The radar used for the measurements is shown in the simplified block diagram, Fig. 1. The transmitter was a conventional X-band pulsed system with the following characteristics: carrier frequency 9225 Mc, prf 500 cps, pulse width 1 μ sec, beamwidth 3 degrees, and peak power 50 kw. The transmitted polarization could be made vertical, horizontal, right circular, or left circular by choice of waveguide components.

The receiver used a four-component polarization resolver (1,2), which resolves the return into vertical, horizontal, right-circular, and left-circular components. This permits simultaneous sampling of four polarized components. Ganged rf attenuators in each of the four channels maintained the signal in the linear range of the receiver. In addition to these four components, two quadrature linear channels at 45 degrees to the horizontal were generated in the rf section. These were used in combination with the vertical and horizontal components for examining the tilt angle (2,3). The transmitter and receiver were optically pointed at the targets.

The six rf signals were separately mixed, amplified at 30 Mc, and detected by conventional methods. The video outputs of the V, H, R, and L channels were stretched, filtered, modulated, and recorded on magnetic tape. The video signals were also fed to a four-channel gray wedge pulse-height analyzer (4,5) which produces the amplitude-distribution density of groups of received pulses. This information may be used in the calculation of statistical properties of the target.

Each channel of the receiver had a dynamic range of 30 db. Errors of ± 1.5 db were observed. These were due in part to the lack of a good afc system and dissimilarities in the i-f response of the various channels.

The photographs from the gray wedge analyzer are seen to have unequal vertical deflections, when the data indicate that these heights should be equal. This corresponds to a calibration error and is due to varying spectral characteristics of the cathode-ray tubes used. This was not detected by the photomultiplier used to set the brightness levels. It will be observed that the vertical channel exhibits low intensity consistently, while the left-circular channel is always high in intensity. This difference, however, will not affect the calculation of the mean voltage from these plots.

EXPERIMENTAL DATA

Ships and Aircraft (Unclassified)

Figure 2 shows the amplitude-time function for a 60-second observation of a barge (range about 9450 yards). Right-circularly polarized illumination was used. The reflected components are, from top to bottom: vertical, horizontal, right circular, and left circular. Here the right-circular return (same polarization sense) is small in comparison with the left-circular return (opposite polarization sense). The properties of the target - a long, flat surface at the viewing aspect - disclose the reversal of polarization sense associated with a single reflection. Since the target is large, even small motions impart rapid changes in the return amplitude. In all the amplitude-time plots, an echoing-area calibration is included. The power-density spectrum of the received left-circularly polarized component during a five-second interval of the run is shown in Fig. 3. Although the target velocity is low, it is seen that the spectrum contains significant components to 25 cps. In the other examples, employing ships with presumably greater velocity, the spectrum may not be higher. A representative photograph of amplitude-distribution density is shown in Fig. 4. These photographs depict, within a time interval (ten seconds in this case), the relative frequency with which amplitude within certain ranges occurred. The abscissa plots received voltage and the ordinate relative occurrence frequency. No outstanding reflective feature is observed since the traces are generally smooth. The height and width of the vertical and right-circular traces, respectively, are distorted due to exposure inaccuracies in the interim system employed.

Figure 5 depicts the return from a tanker (range approximately 16,000 yards). Right-circularly polarized transmission was employed. This time the same sense component (right circular) as transmitted contains significant amplitudes. Thus the double-bounce mechanism, producing two polarization sense reversals, is prominent. Several regions are observed where the signal fluctuations are very slow. Assuming that the ship was in continuous motion, a possible explanation is the large corner formed by the deck and superstructure, which was visible from the observed aspect angle. Subsequent observations of this target disclose the same general appearance in the return. Since much of the variation in the polarization channels appears closely correlated, the primary mechanism is a fluctuation in backscattered power rather than gross changes in polarization. Certain segments, such as the interval between 70 and 90 seconds, however, do exhibit significant variation in return polarization, as evidenced by fading in one channel accompanied by peaking in another. Figure 6 shows the power-density spectra of the received right- and left-circularly polarized channels during the 80 to 85 second interval of the run. Figure 7 shows photographs of amplitude-distribution density. Figure 7a was taken during the early part of the run (70 to 80 seconds) and shows no prominent peaks, since the target area is smoothly distributed. Figure 7b, taken during the interval 130 to 140 seconds, shows rather prominent peaks associated with discrete reflectors. It is to be noted that this occurred just after the broad response was observed. Side-lobe reradiation from the target is a possible explanation.

Figure 8 shows the data received when a freighter was illuminated with vertical polarization (range about 7900 yards). Here the target is high out of the water and is complex, so that no single corner-like feature predominates. Although no crosspolarization is observed (horizontal equal to zero, right and left circular equal in detail), this does not necessarily mean that illumination with some other polarization would also result in no crosspolarization. (See Appendix A, Ref. 2.) Figure 9 shows the power-density spectrum of the vertically polarized return. Since no crosspolarized return occurred, the right- and left-circularly polarized components are identical. Figure 10 shows the amplitude-distribution density. The target is complex and presents a smoothed distribution. Figure 11 shows the return when illuminating a fleet tug with right-circular polarization (range 9200 yards, water surface smooth). This target is large and complex. The return discloses many uncorrelated peaks in the receiver channels, hence substantial depolarization is occurring. At about 25 seconds a low-frequency region is observed. The center of this region shows predominantly opposite sense (left-circular) return polarization, while the overall section contains prominent side lobes. The mechanism is that of a flat plate turning slowly.

Figure 12 depicts the spectrum of the left-circular component for a five-second interval. Significant components are observed to about 17 cycles. The amplitude-distribution-density photograph (Fig. 13) again discloses a smoothly distributed target over the interval shown (10 to 20 seconds).

The power spectra in this report are, for the most part, short time samples compared with the lowest frequency contained in the signal; hence resolution of low frequencies is not possible. The short time interval used will show the higher frequencies on the signal which would not be seen for a long sample, since the power in these frequencies is small compared with the low-frequency power. An example of this variation in apparent power spectrum with sample length is shown in Figs. 12 and 14. Figure 12 shows frequencies to 17 cps for a five-second data sample, while Fig. 14, a 50-second time interval of the same run, including the five seconds analyzed in Fig. 12, shows frequencies to only 1.7 cps. The true power spectrum would be one which did not change appreciably as the sample length is increased.

The return from a propeller aircraft is shown in Fig. 15. This figure shows the return from a twin-engine aircraft (Convair type 240) with vertical polarization transmitted. The aircraft was inbound on a crossover course at about 12,350 yards. The only depolarization observed is that due to propeller modulation, which the frequency analysis in Fig. 16 shows to be 45 cps, and it appears in the horizontal return. From the propeller modulation observed, the engine speed of the aircraft can be determined: frequency (cycles/min) \times engine-to-propeller gear ratio/number of prop blades: $(45)(60)(20/9)(1/3) = 2000$ rpm. The engine rpm specified for this aircraft is 2100 rpm at cruising speed. Horizontal polarization from the propeller is occurring because of the aspect angle of the propeller with respect to the radar line of sight. Since the angle is not 90 degrees, the propeller appears unsymmetrical, producing a net horizontal return three times for each complete propeller revolution. The propeller modulation described above is not seen in vertical return, due to the greater low-frequency power returned from the airframe at the aspect angles observed. The power received at this frequency is in excess of 16 db down from the low-frequency power and is out of the range of the spectrum analyzer.

Sea Return, Chaff, and Operational Aircraft (Secret)

A single-engine aircraft, probably a T-28, illuminated with right-circular polarization, is shown in Fig. 17. The aircraft was observed flying away from the radar, range about

8600 yards. Propeller modulation is also observed in this run, prominently in the vertical, horizontal, and left-circular returns. Depolarization is observed, since reflections between the wing and tail surfaces and the fuselage cause a double reflection and return energy in the same sense as transmitted. Propeller modulation occurs in the same sense only for a small range of aspect angles. The frequency spectrum of this run (Figs. 18, 19) shows that the right-circular return contains only very low frequencies, while the left return is predominantly composed of the propeller chopping frequency. Signal levels for these runs were too low to provide suitable gray wedge photographs for analysis.

Figure 20a, b, and c shows the return from an F3H aircraft flying in a crossing course at about 400 knots; crossover range was about 6300 yards. Illumination was right-circularly polarized, and the aircraft was dispensing chaff* regularly during the flight. The three figures depict the same run, but with different recorder chart speeds. Figure 20a, which shows about 40 seconds of the run, discloses a reflection from a prominent surface, perhaps the wing edge or cockpit canopy, at about 42-1/2 seconds, one of the chaff drops at 50-1/2 seconds, and crossover at about 63-1/2 seconds. Since the radar was tracking the aircraft, the chaff appears only for a brief interval. Figure 20b and c depict expanded looks at the same data. The reflection at 42-1/2 seconds appears as all opposite-sense (left-circular) polarization, so that a flat surface rather than an edge (which would produce a substantial linear component) is involved.

Figures 21 and 22 show two sections of another run using the same F3H, again dispensing chaff. At 19 seconds (range 10,800 yards) chaff was dropped; the return shown was again obtained with right-circularly polarized illumination. Figure 22 shows the region just prior to crossover (which occurred at about 60 seconds). At about 36 seconds a reflection (corresponding to the one at 42-1/2 seconds in the run of Fig. 20a) occurred. At about 51 seconds chaff was again dropped, producing the marked change in the return. The change in time scales used in the charts is to be noted. At 97 seconds chaff was again dropped.

Power-density spectra obtained during crossover (57 to 62 seconds) is shown in Fig. 23 for the four received components. Figure 24 shows the gray wedge plot obtained during crossover with this aircraft.

Figure 25 shows a 13-second sample of sea return. The range was 2100 yards, and the depression angle about one degree. The water surface was rough, and in general this condition was necessary to obtain significant return with the system. Left-circularly polarized illumination was used. Power-density-spectrum plots are shown in Fig. 26. These plots show the power-density spectrum of two seconds of the 13-second run shown in Fig. 25. A gray wedge photograph from a ten-second radar-return sample is shown in Fig. 27.

It is to be noted that the general appearance of the sea return and chaff drop is similarly noisy. It is instructive to compare their characteristics. To facilitate comparison, a one-second sample of the sea return was re-recorded using a high-speed three-channel oscillograph (Fig. 28). Since the oscillograph drive did not hold speed very well in the interval, two records are shown, from which corresponding amplitudes may be obtained from the four channels. The vertical lines were drawn to indicate corresponding instants of time.

*Single packages of chaff were pneumatically dispensed. The chaff itself consisted of aluminum-coated glass-fiber dipoles in lengths varying from 9/16 to 3/4 in.

A re-recording of a one-second portion of the chaff drop shown in Fig. 21 was made using the same high-speed oscillograph and is shown in Fig. 29. Speed uniformity here permitted the combination of two records in a single photograph. Figure 30 shows the power-density spectrum of a two-second sample of data in Fig. 21. The samples in Figs. 28 and 29 were fitted to a computer program, and the autocorrelation, power spectrum, and crosscorrelation of the various components were derived.

AUTOCORRELATION AND CROSSCORRELATION FUNCTIONS (UNCLASSIFIED)

Computation was made on the NRL-Narec computer utilizing the one-second interval of data from each of the two runs. Computation was actually carried out on the basis of the autocovariance and covariance of functions, and the resultant data were normalized to obtain the autocorrelation and crosscorrelation function. For example, given a time function, $f_1(t)$ over an interval T , we find for the autocovariance (6):

$$C_{11}(\tau) = \left\langle [f_1(t) - \bar{f}_1] [f_1(t + \tau) - \bar{f}_1] \right\rangle_T \quad (1)$$

where \bar{f}_1 is the average value of $f_1(t)$ over the interval T . The normalized autocovariance (6) or the autocorrelation then becomes

$$\phi_{11}(\tau) = \frac{C_{11}(\tau)}{C_{11}(0)}. \quad (2)$$

To compute the covariance and crosscorrelation functions, the following technique was employed. Given $f_1(t)$ and $f_2(t)$, with mean values \bar{f}_1 and \bar{f}_2 in the interval employed, the covariance is defined:

$$C_{12}(\tau) = \left\langle [f_1(t) - \bar{f}_1] [f_2(t + \tau) - \bar{f}_2] \right\rangle_T \quad (3)$$

The crosscorrelation is then obtained from

$$\phi_{12}(\tau) = \frac{C_{12}(\tau)}{\sqrt{C_{11}(0) \cdot C_{22}(0)}}. \quad (4)$$

In the definitions given, subtracting out the mean value of the sample serves to prevent the detail in the random or periodic component from being suppressed when plotted after normalization.

CORRELATION FUNCTIONS OF POLARIZED COMPONENTS (SECRET)

The mean value will always exist in these measurements, because its presence represents some finite scattering area which, after all, is the radar target. The normalization quantity $C_{11}(0)$ is then just the ac component of power in the radar return.

In any single channel the returns represented in Figs. 28 and 29 show variations with time. Given just the single-channel output, as obtained from the usual radar, for example, the source of the variations - i.e., power fading or amplitude trade-off between a pair of channels - is not disclosed. In the present system pairs of amplitude channels are available, and it is instructive to compare their variations. Little will be said of the autocorrelation functions, since their interpretation is widely understood.

The crosscorrelation function of interest here is the correlation between the orthogonal components of the received wave in each of the wave bases, i.e., $\phi_{\text{VH}}(\tau)$ and $\phi_{\text{RL}}(\tau)$. Components such as $\phi_{\text{VR}}(\tau)$ and $\phi_{\text{HL}}(\tau)$ are of little utility, since some redundancy is always present ($P = V^2 + H^2 = R^2 + L^2$), and some degree of crosscorrelation will always occur. Moreover, since there are component waves received from the same target, their degree of correlation at $\tau = 0$ (the unlagged value) is of primary importance. Considering then the value of the crosscorrelation function at the origin, $\phi_{12}(0)$, between the orthogonal components of the incoming wave, several conclusions may be drawn concerning the nature of the radar return.

If the value of $\phi_{12}(0)$ is large and positive, obviously variation in the received wave power is occurring.* On the other hand, wave polarization is defined in terms of the ratio of the two orthogonal components, so that polarization changes as a function of time are "suppressed" under this condition.

If $\phi_{12}(0)$ is large and negative, then increases in signal amplitude in one channel are accompanied by decreases in the orthogonal component channel, and conversely. This type of performance tends toward more uniform power, but at the same time the polarization ratio must change.* If the average values of the functions are comparable with the peak-to-peak deviations, the polarization ratio can vary through extreme values; in the limit, it approaches power fading in one polarized channel accompanied by re-emergence of the power in the orthogonally polarized channel.

Under some circumstances the crosscorrelation may be very low, perhaps even zero. For this observation interval, then, there are some of each of the conditions described above occurring. Hence no statement may be made concerning the power variation over the interval, although it is evident that under these conditions the polarization ratio does not remain constant. The lack of correlation between these two quantities, which are components of the total received signal, may itself be significant.

In the present system two sets of components are available, i.e., one pair of orthogonal linears and the orthogonal circulars. If crosscorrelation between the components of one set is compared with crosscorrelation between the components of the other set there will, in general, be some differences. These differences are due to inclusion of phase data in one pair of components which is not included in the other.† If there is little difference, and if the average values are similar, then polarization is seen to approximate linear with a tilt angle of 45 or 135 degrees (the condition for $H = V = R = L$).

*The amount of variation is, of course, a function of the average values which have been subtracted off for purposes of this analysis.

†Given the pair E_L and E_R with a phase difference θ , the circular channels indicate $|E_L|$ and $|E_R|$; however, the linear channels indicate

$$|E_V| = \sqrt{|E_R|^2 + |E_L|^2 - 2|E_R E_L| \cos \theta}$$

$$|E_H| = \sqrt{|E_R|^2 + |E_L|^2 + 2|E_R E_L| \cos \theta}.$$

INTERPRETATION OF COMPUTED RESULTS (SECRET)

Figure 31 shows the power-density spectra derived from the computer program for the chaff sample. The effective resolution of the spectrum is about ten cycles. A two-second sample which included the data used for computation was analyzed with the scanning analyzer set with an effective resolution of about 15 cycles. The results are shown in Fig. 30. It is seen that the water-surface return contains a significantly lower signal spectrum than the chaff (Fig. 32). The crosscorrelation characteristics, shown in Figs. 33 and 34, also reveal substantial differences. The water surface shows fair positive correlation between components of both the linear and circular pairs, indicating power fading to be a prominent characteristic. On the other hand, the chaff shows nearly zero crosscorrelation (for $\tau = 0$, which is rather unique in itself). Polarization variations during the interval are perhaps the dominant characteristic.

It should be noted that the simultaneous four-channel reception will lead (assuming target characteristics are favorable) to significant values of crosscorrelation. On the other hand, independent runs with the various polarizations would not show these results except for a fortuitous set of circumstances. In general, the results would appear similar to Figs. 33 and 34 at the larger lagged values.

CONCLUSIONS (SECRET)

A variety of targets have been examined using the omni-polarized receiver system, in conjunction with various transmitter polarizations. Generally, when linearly polarized transmission is used, the signal-return variations are traceable to "power fading" rather than polarization changes. Propeller modulation, however, induces significant cross-polarization. With circular transmission, crosspolarized components occur readily, since the complex nature of the targets permits many multiple wave reflections.

An analysis of the radar return from two noisy targets, chaff and sea water, reveals that chaff return contains both polarization and power changes, whereas the sea return discloses mostly power changes.

ACKNOWLEDGMENTS (UNCLASSIFIED)

The authors wish to thank A. E. March and D. C. Hut for their work in the fabrication and testing of the radar system and assistance in data reduction. The work of H. G. Thompson and B. E. Wittman in determining the mechanical designs and directing the trailer modifications to accommodate the radar system is appreciated.

The contributions of the members of the New Techniques Section, Tracking Branch, Radar Division, for the initial design and testing of many of the components in the microwave system and in the many valuable suggestions is acknowledged.

The computer programming was the work of C. G. Myers of the Terminal Equipment Section of the Tracking Branch, and his help is greatly appreciated.

REFERENCES

1. Allen, P.J., and Olin, I.D., "A Four-Component Polarization Resolver for Microwaves," NRL Memo. Rept. 1086, Apr. 1960
2. Olin, I.D., and Queen, F.D., "Measurements Using a Polarization Instrumentation Radar on Navigational Buoys," NRL Report 5701, Nov. 1961
3. Olin, I.D., "A System for the Dynamic Measurement of Radar Return Polarization," NRL Memo. Rept. 1082, Apr. 1960
4. Olin, I.D., "An Automatic Amplitude Distribution Recorder," Transactions of the 1959 Symposium on Radar Return - Part I, NOTS TP2338, pp. 145-168, May 11-12, 1959
5. Bernstein, W., Chase, R.L., and Schardt, A.W., "Gray Wedge Pulse-Height Analysis," Rev. Sci. Instr. 24(6):437-444 (1953)
6. Blackman, R.B., and Tukey, J.W., "The Measurement of Power Spectra from the Point of View of Communications Engineering," Bell System Tech. J., Vol. 37, Part I, pp. 185-282, Part II, pp. 485-569, Jan., Mar., 1958

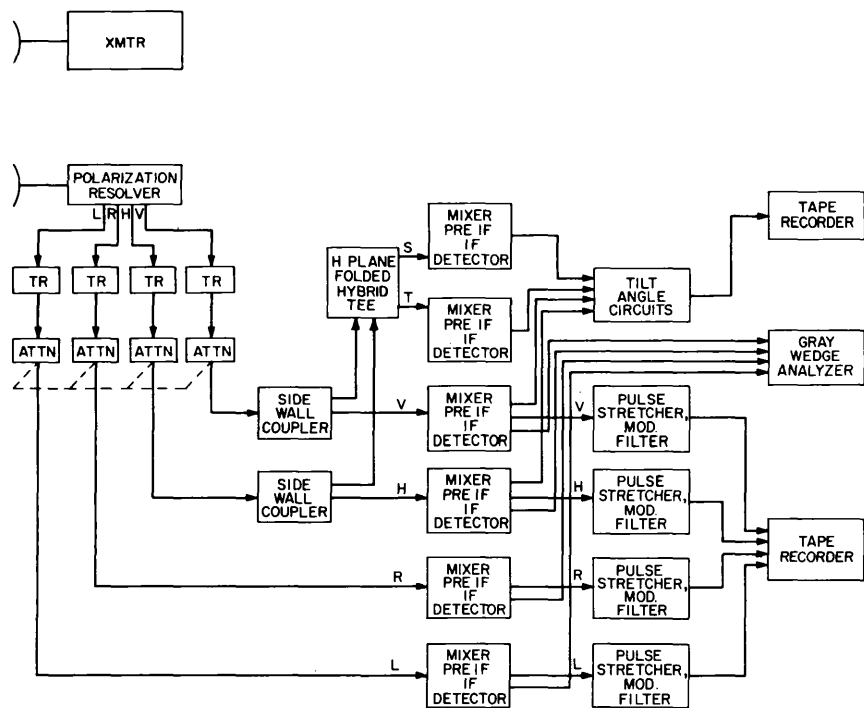


Fig. 1 - Simplified block diagram, polarization radar
(Unclassified)

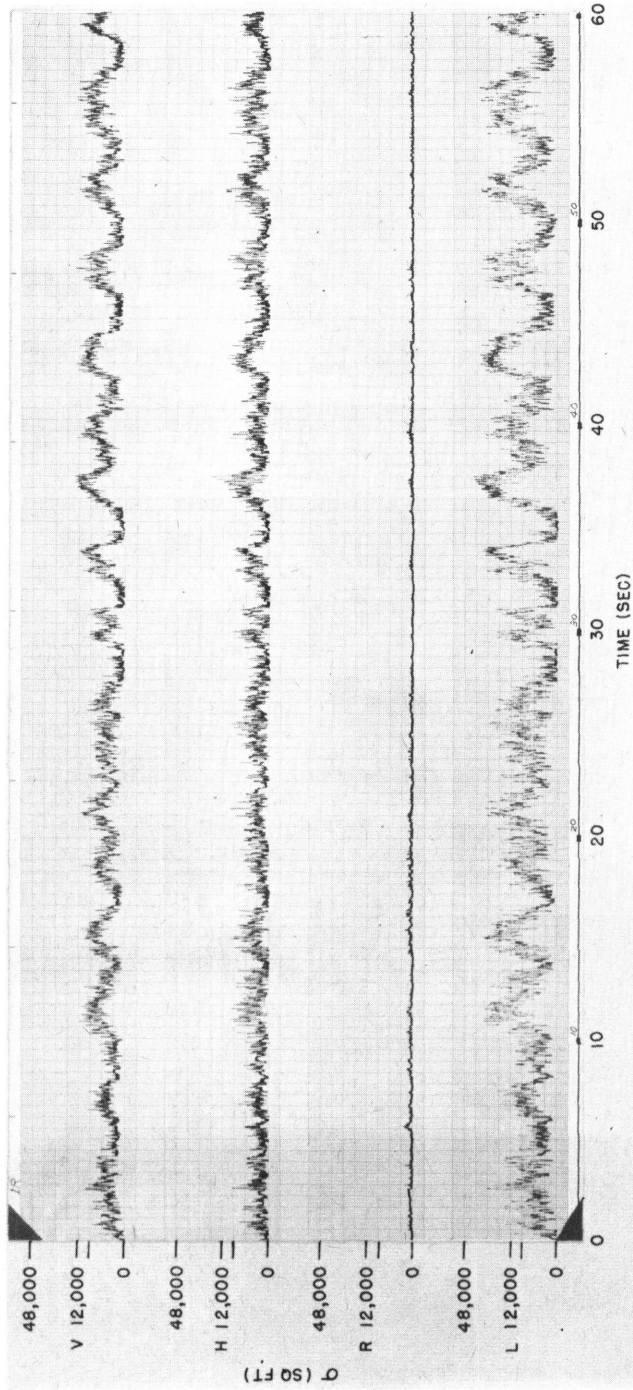


Fig. 2 - Run IR, barge, range 9450 yards, right-circular polarization transmitted (Unclassified)

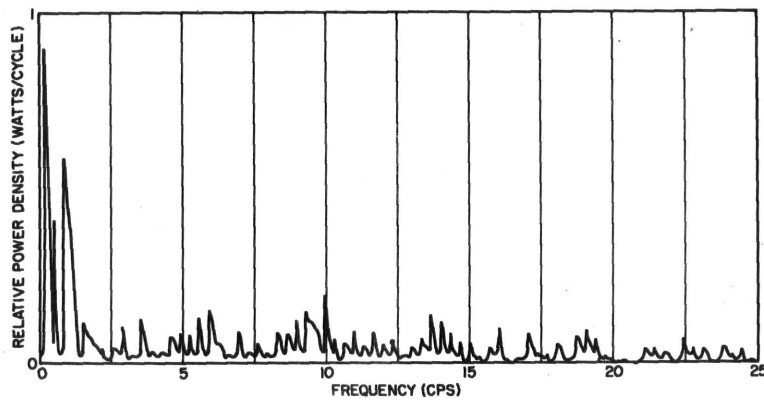


Fig. 3 - Run 1R, barge, transmitted polarization right circular, received left circular, time interval 5 to 10 seconds (Unclassified)

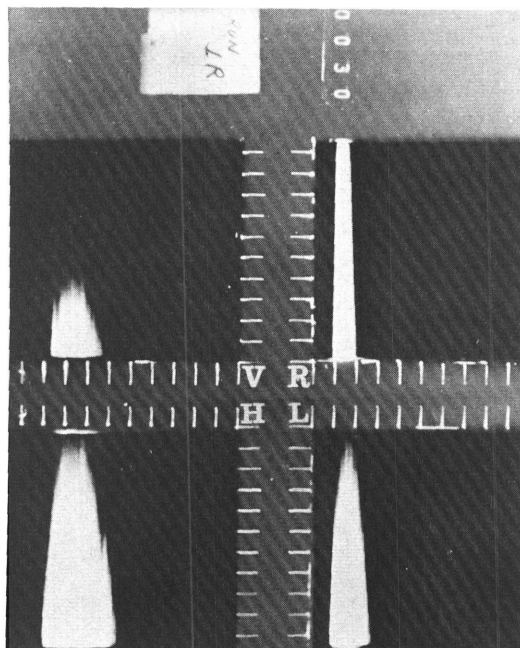


Fig. 4 - Echo-amplitude distribution density for the 20 to 30 second time interval of run 1R. The abscissa plots received voltage and the ordinate relative occurrence frequency (Unclassified)

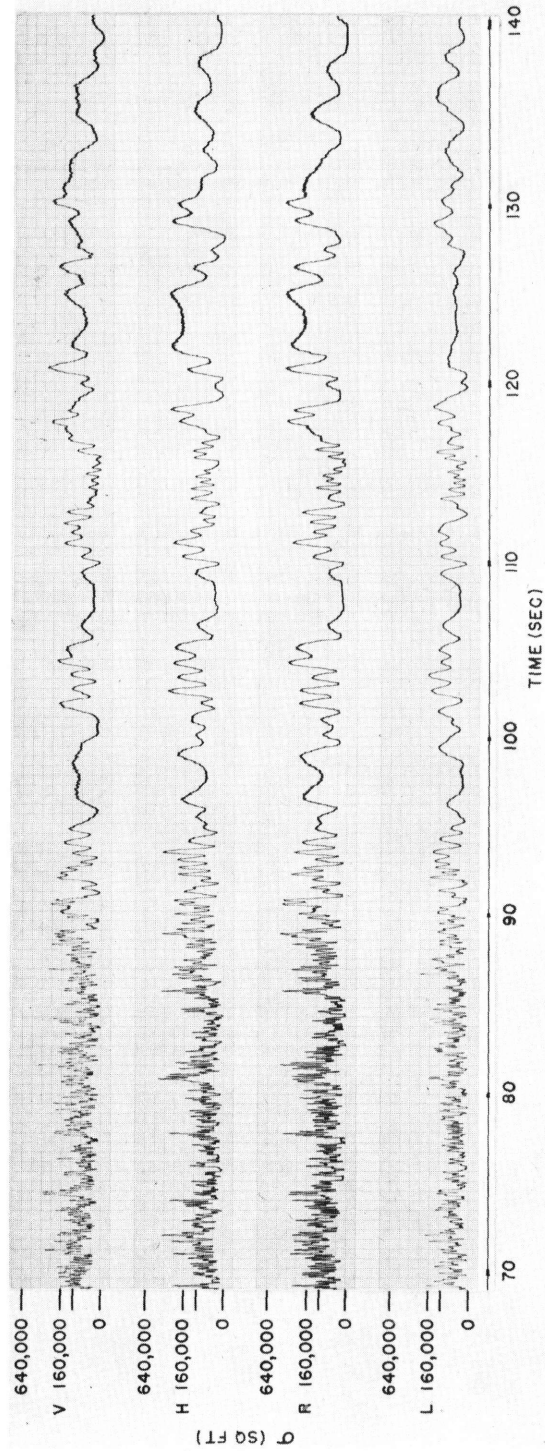
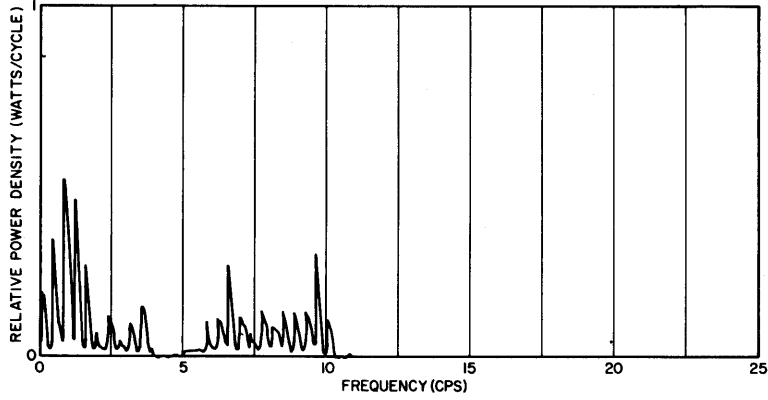
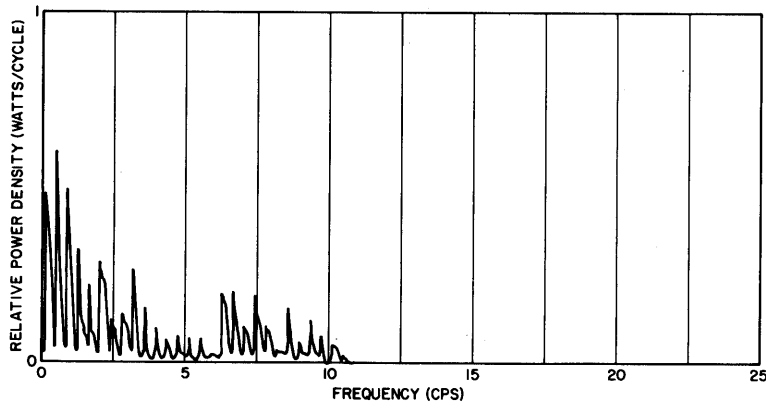


Fig. 5 - Run 25R, tanker, range 16,000 yards, transmitted, polarization right circular (Unclassified)

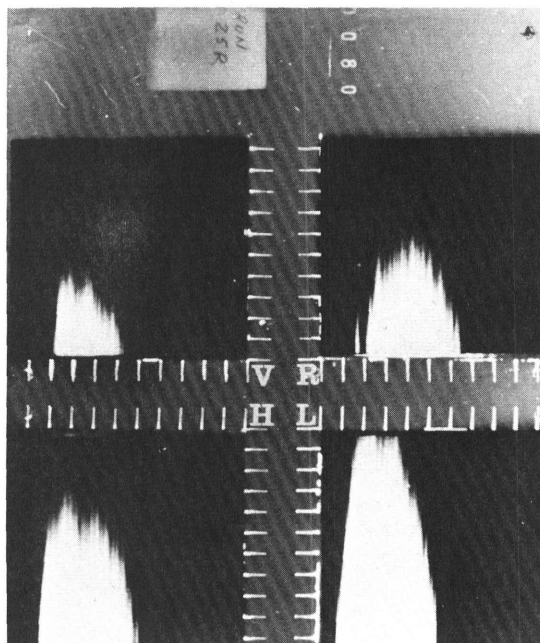


(a) Received right circular



(b) Received left circular

Fig. 6 - Run 25R, tanker, transmitted polarization right circular, time interval 80 to 85 seconds (Unclassified)



(a) Time interval 70 to 80 seconds

(b) Time interval 130 to 140 seconds

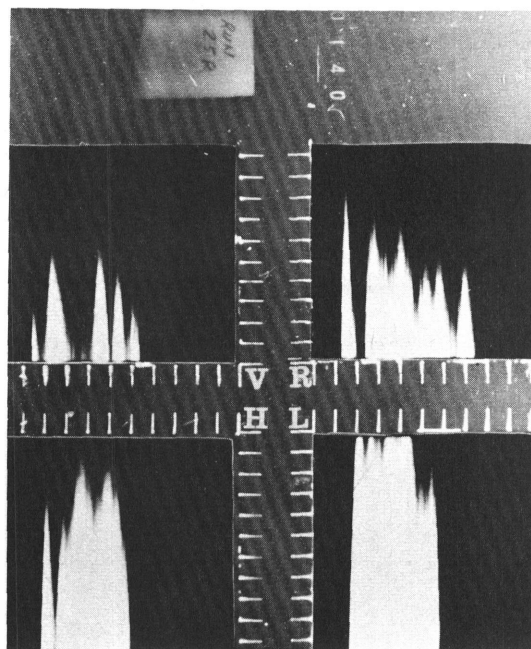


Fig. 7 - Echo-amplitude distribution density for run 25R (Unclassified)

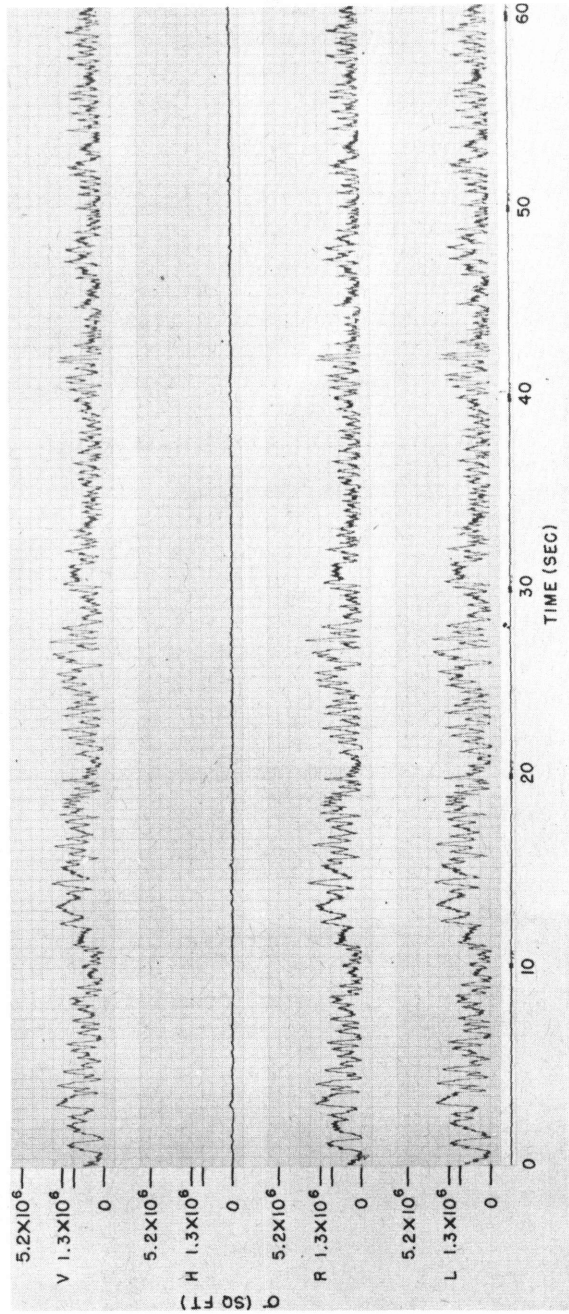


Fig. 8 - Run 13V, freighter, range 7900 yards, transmitted polarization vertical (Unclassified)

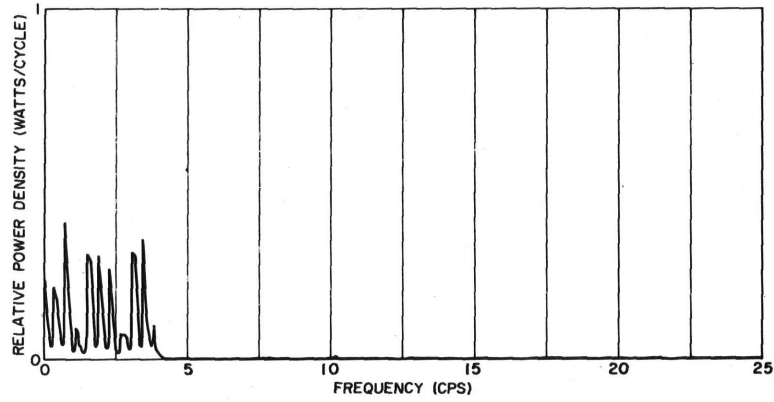


Fig. 9 - Run 13V, transmitted polarization vertical, received vertical, time interval 5 to 10 seconds (Unclassified)

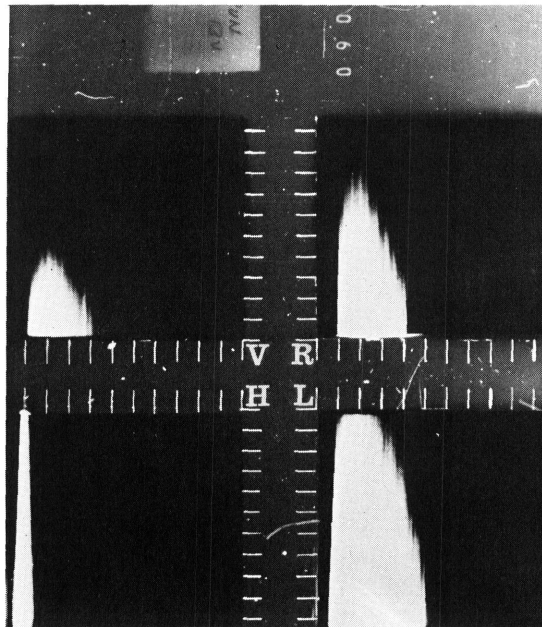


Fig. 10 - Echo-amplitude distribution density for the 50 to 60 second time interval of run 13V (Unclassified)

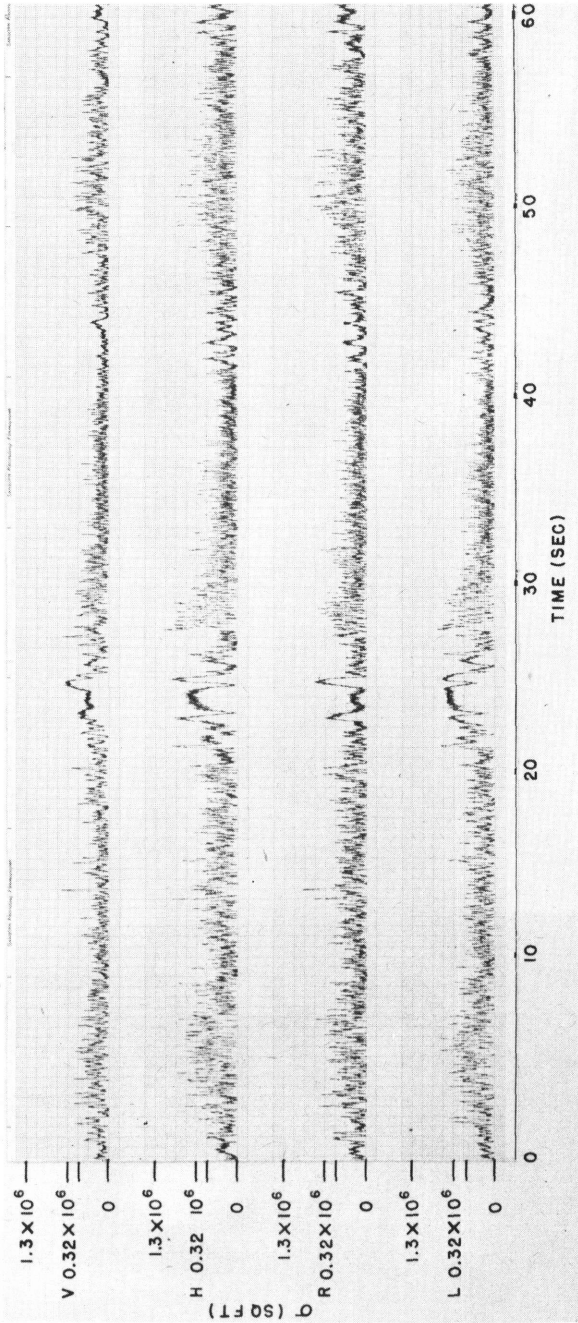


Fig. 11 - Run 6R, fleet tug, range 9200 yards, transmitted polarization right circular (Unclassified)

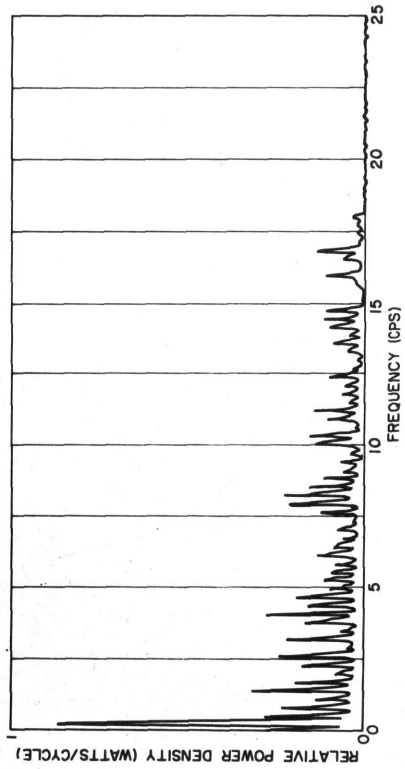


Fig. 12 - Run 6R, fleet tug, transmitted polarization right circular, received polarization left circular, time interval 5 to 10 seconds (Unclassified)

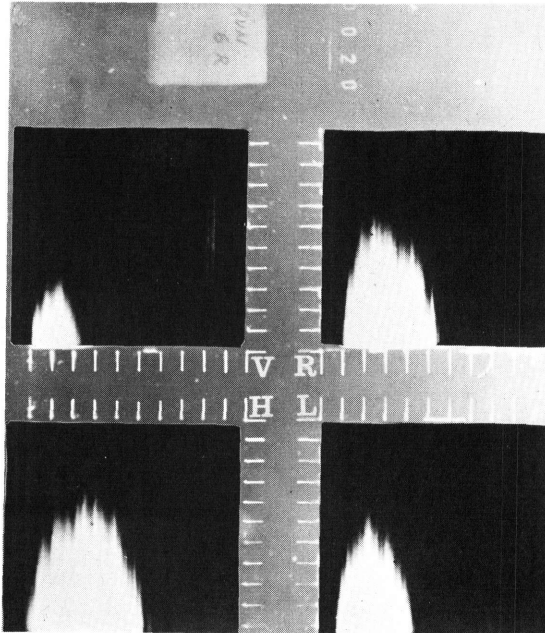


Fig. 13 - Echo-amplitude distribution density for the 10 to 20 second time interval of run 6R (Unclassified)

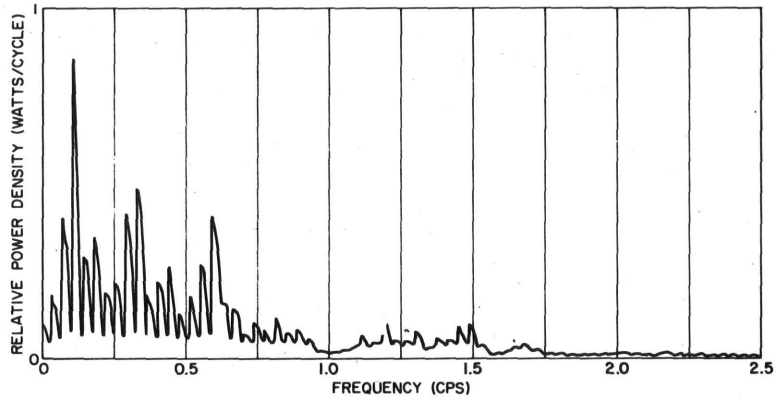


Fig. 14 - Run 6R fleet tug, transmitted polarization right circular, received left circular, time interval 0 to 50 seconds (Unclassified)

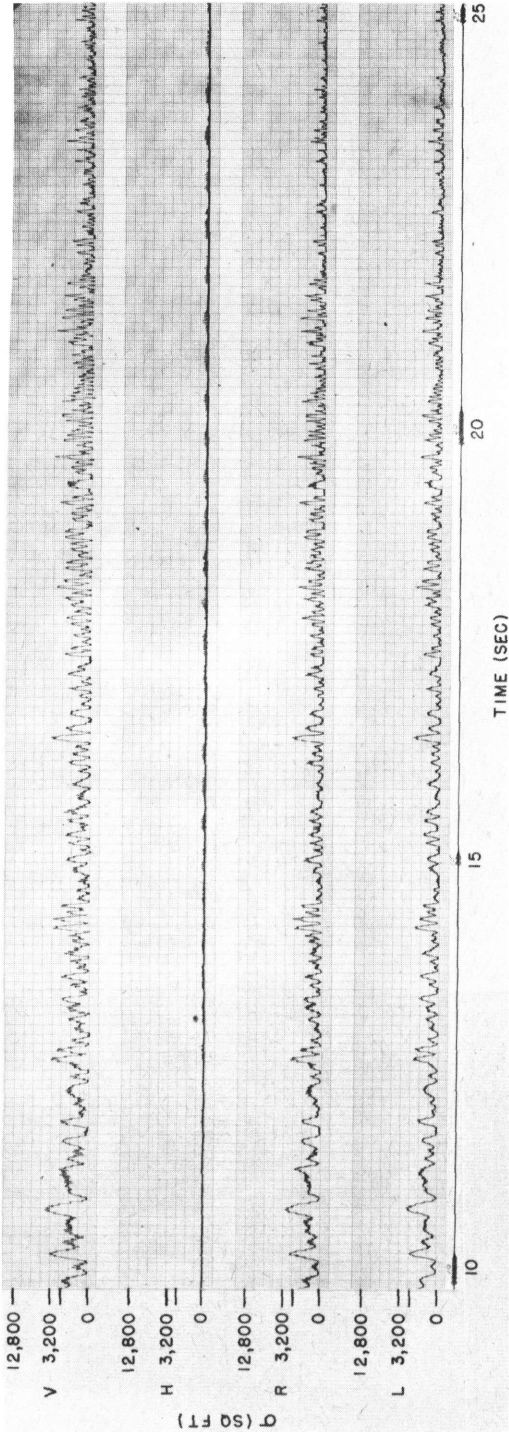


Fig. 15 - Run 22V, twin-engine propeller aircraft, range 12,350 yards, transmitted polarization vertical (Unclassified)

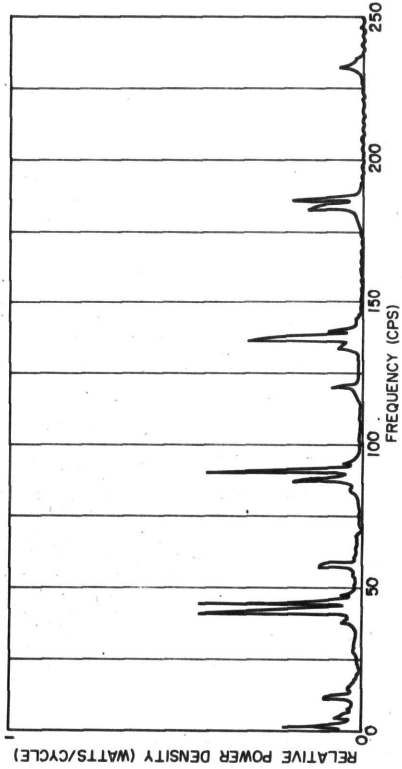


Fig. 16 - Run 22V, transmitted polarization vertical, received horizontal, time interval 15 to 20 seconds (Unclassified)

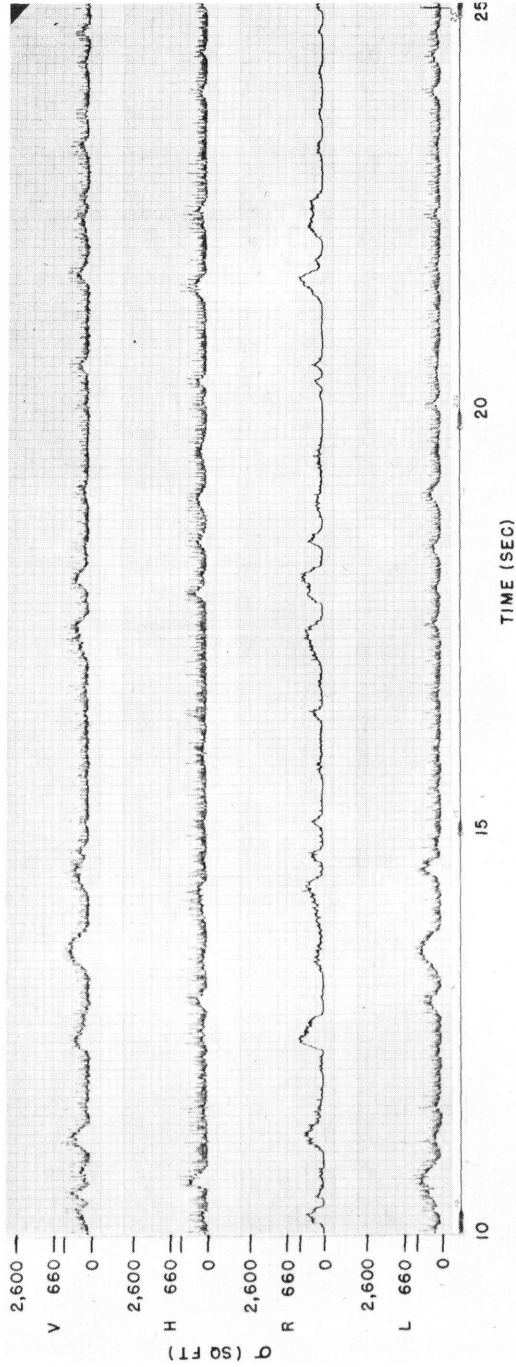


Fig. 17 - Run 24RL, single-engine propeller aircraft, range 8600 yards, transmitted polarization right circular, ordinate calibration at the mean range (Secret)

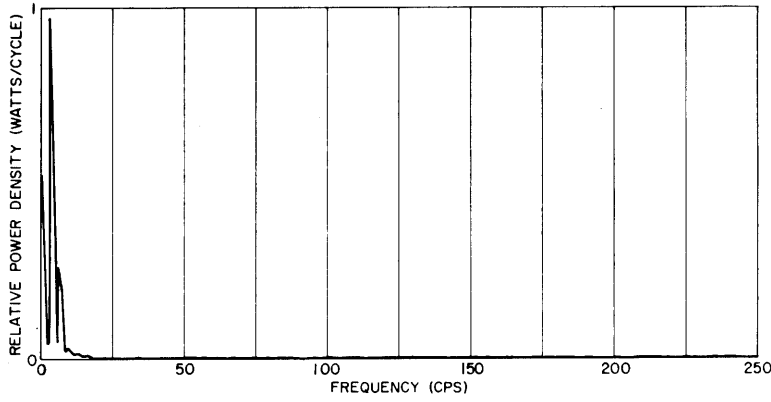


Fig. 18 - Run 24RL, transmitted polarization right circular, received right circular, time interval 15 to 20 seconds (Secret)

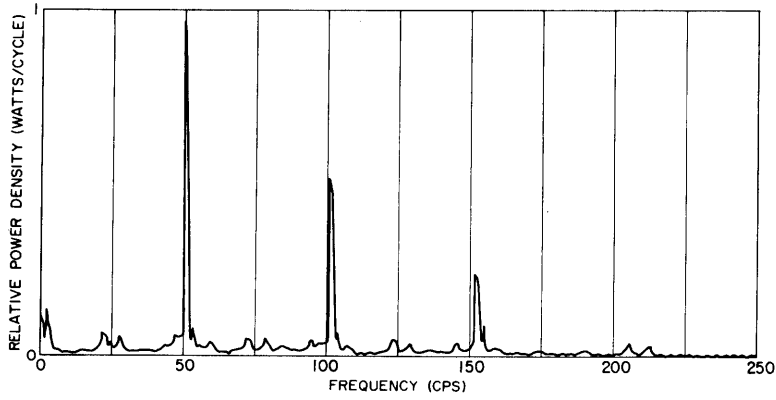
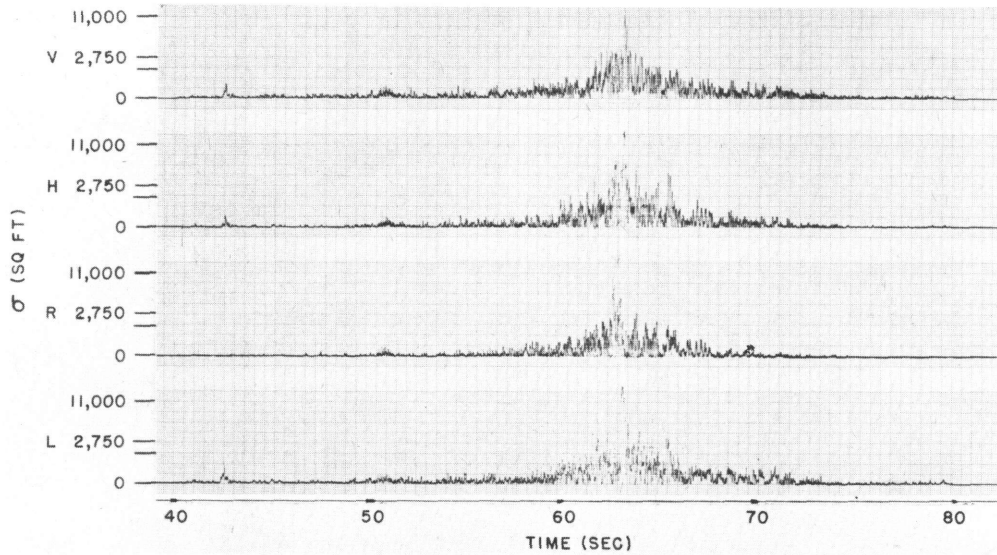
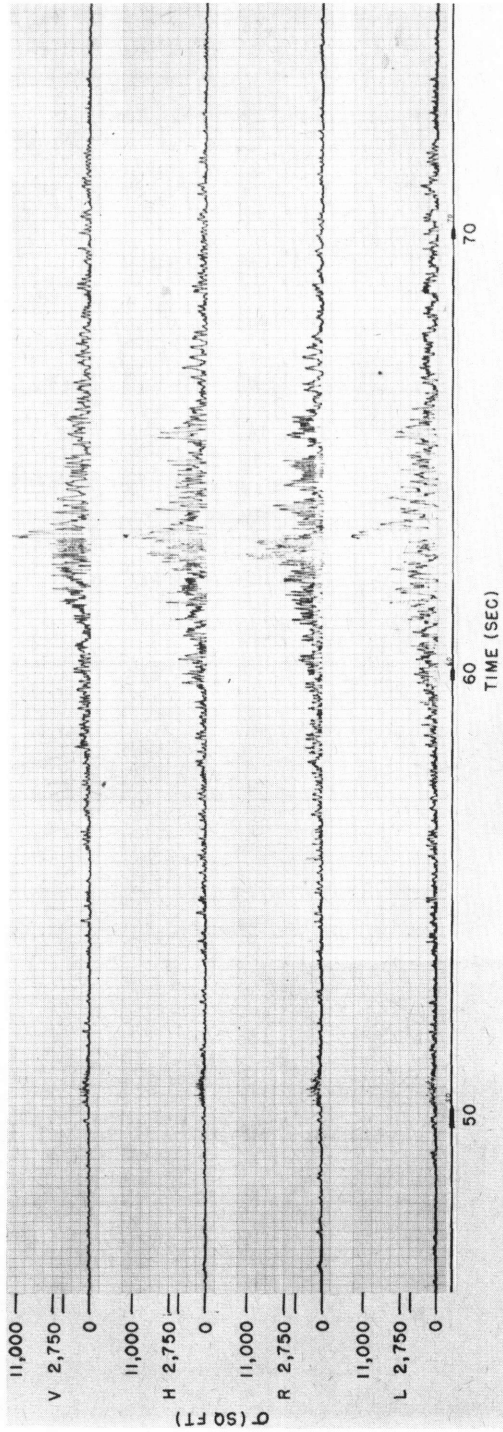


Fig. 19 - Run 24RL, transmitted polarization right circular, received left circular, time interval 15 to 20 seconds (Secret)



(a) Portion of the run which shows aircraft approach, chaff drop, and crossover

Fig. 20 - Run 24RR, F3H aircraft, minimum range 6300 yards, transmitted polarization right circular. Cross-section values listed are for broadside (Secret).



(b) Enlarged portion of the run, showing chaff and crossover

Fig. 20 (Continued) - Run 24RR, F3H aircraft minimum range 6300 yards, transmitted polarization right circular.
Cross-section values listed are for broadside (Secret).

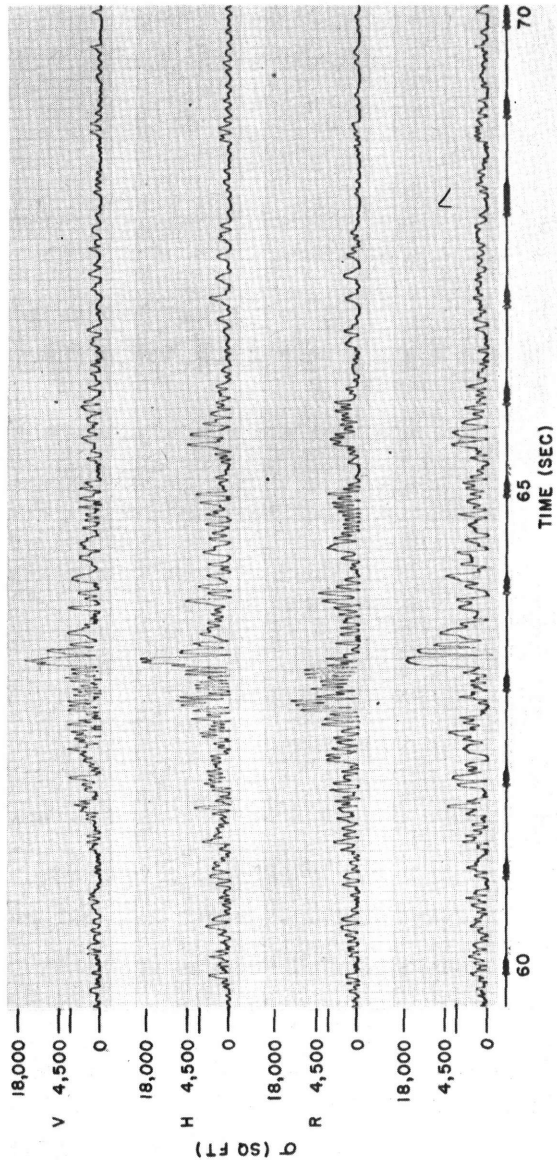


Fig. 20 (Continued) - Run 24RR, F3H aircraft, minimum range 6300 yards, transmitted polarization right circular. Cross-section values listed are for broadside (Secret).

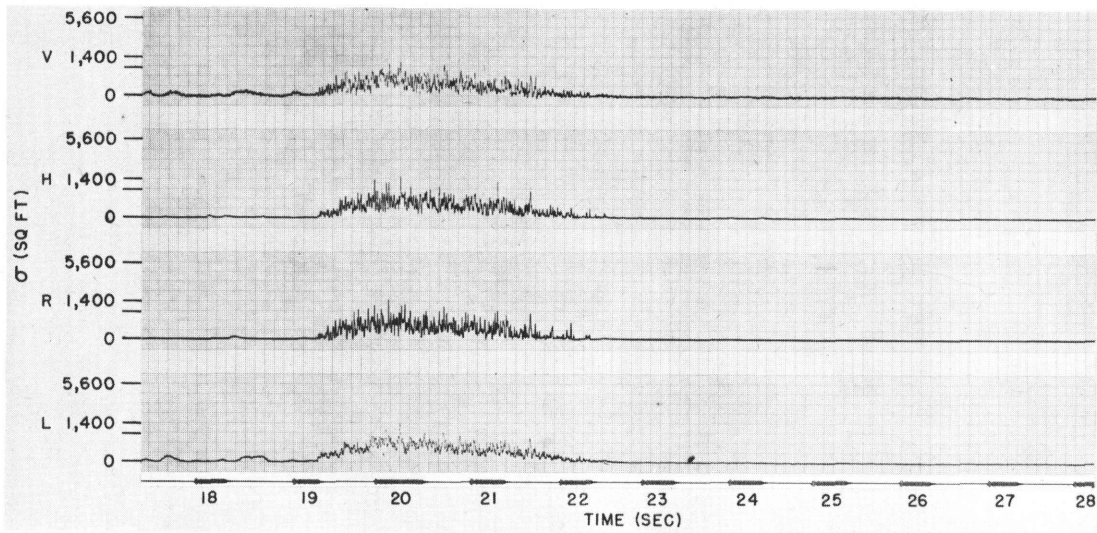


Fig. 21 - Run 24RH, chaff, range 10,800 yards, transmitted polarization right circular (Secret)

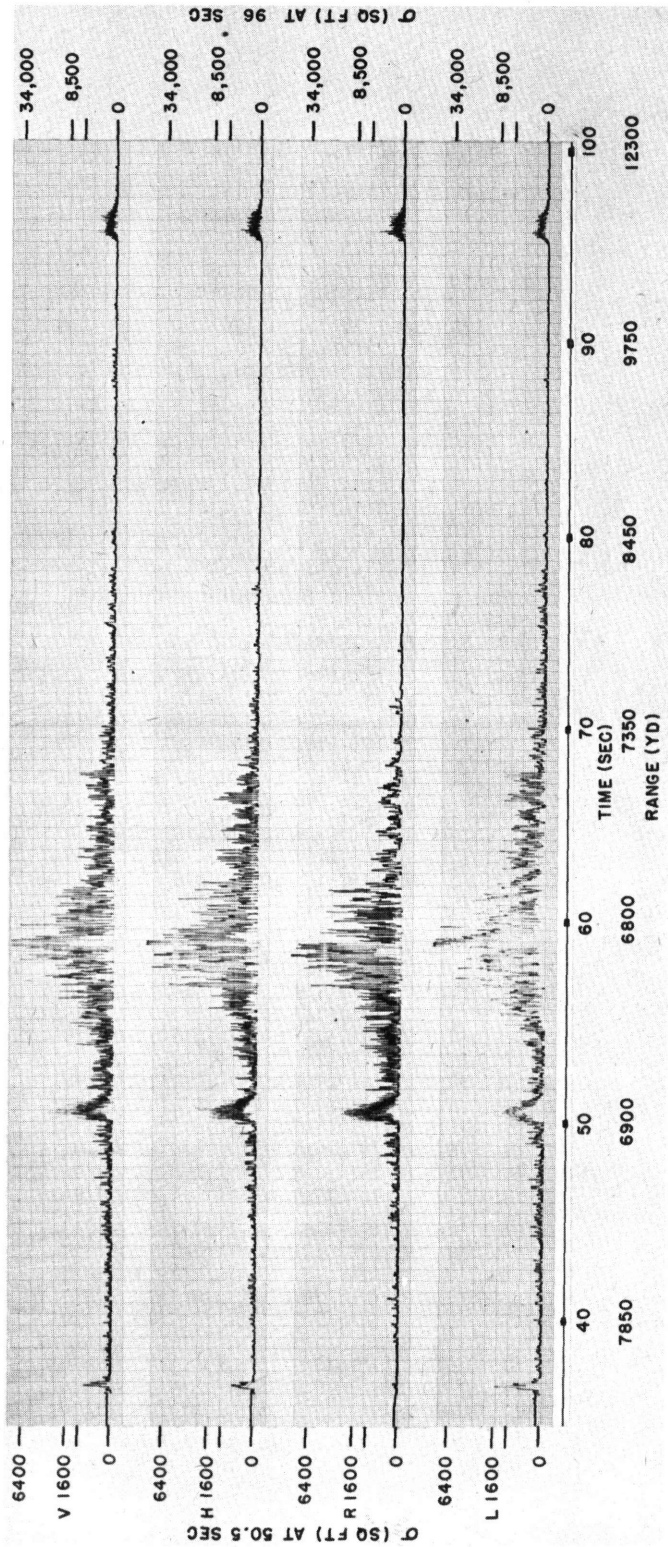
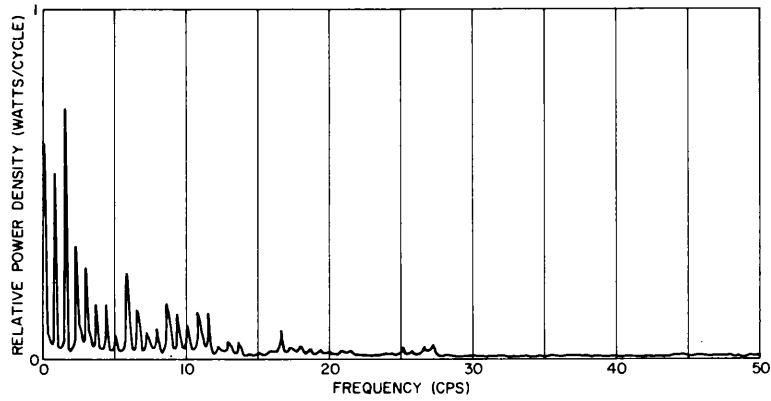
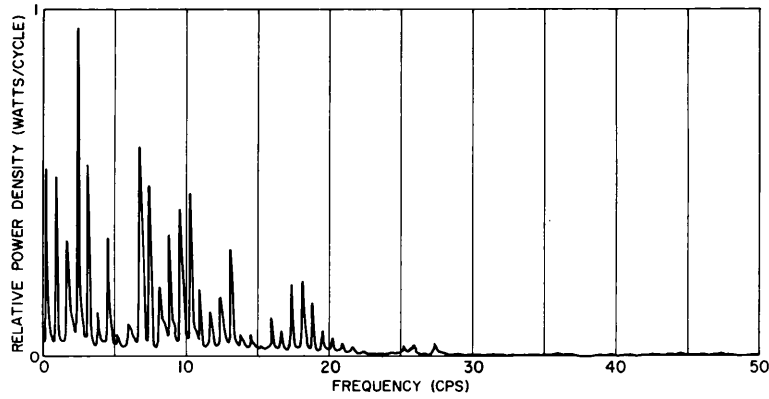


Fig. 22 - Run 24H, F3H aircraft, transmitted polarization right circular. Cross-section values listed are for 50.5 seconds at left and 96 seconds at right of plot. Saturation of data near broadside aspect angles has occurred (Secret).



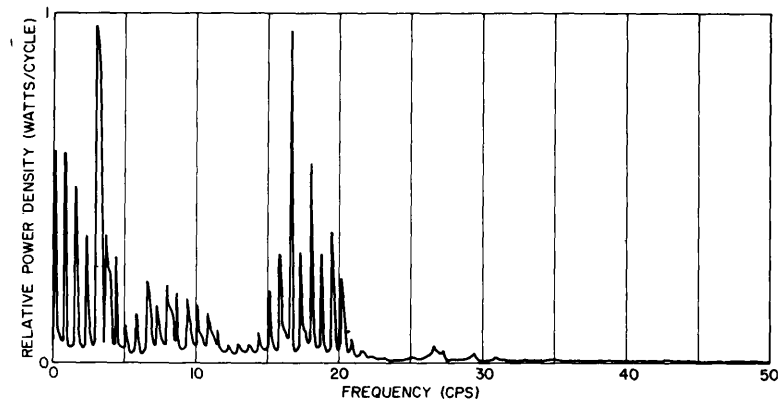
(a) Received vertical



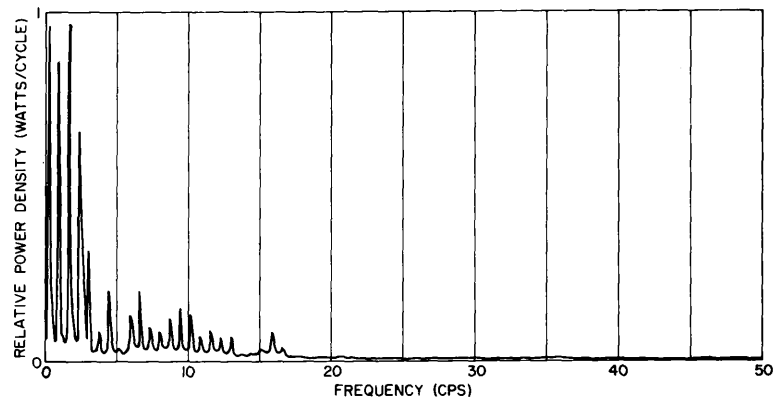
(b) Received horizontal

Fig. 23 - Run 24RH, transmitted polarization right circular, time interval 57 to 62 seconds (Secret)

NAVAL RESEARCH LABORATORY



(c) Received right circular



(d) Received left circular

Fig. 23 (Continued) - Run 24RH, transmitted polarization right circular, time interval 57 to 62 seconds (Secret)

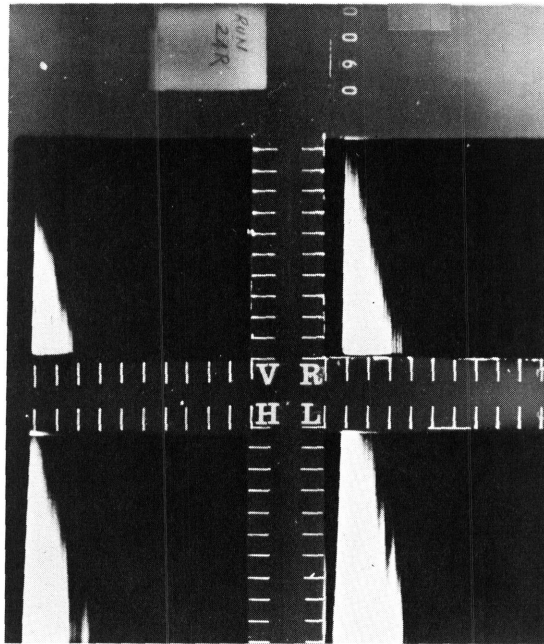


Fig. 24 - Echo-amplitude distribution density for a broadside aspect of run 24R (Secret)

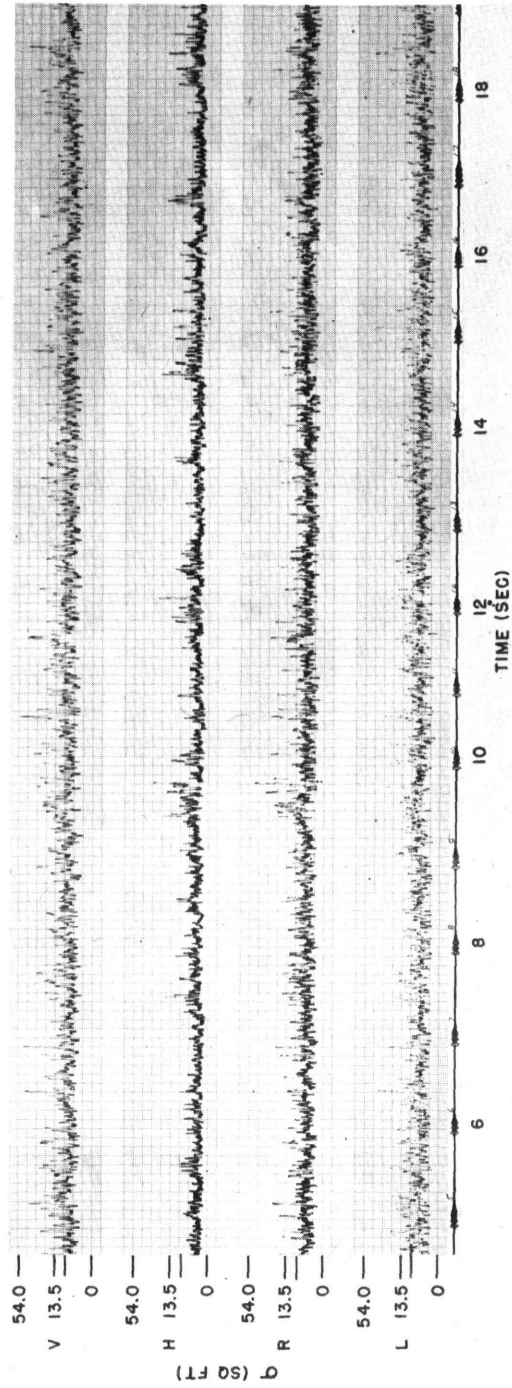
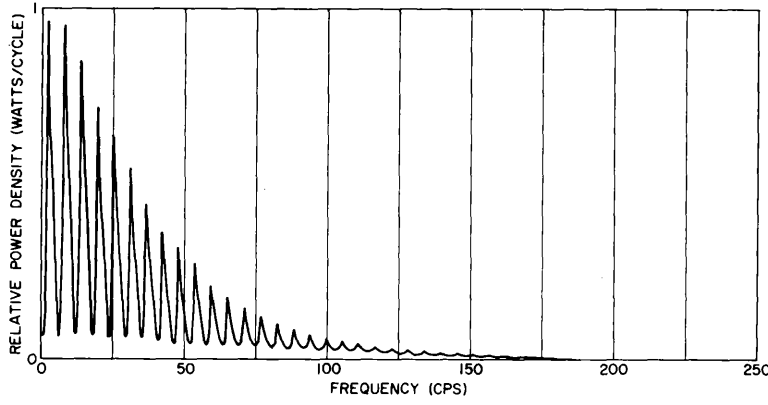
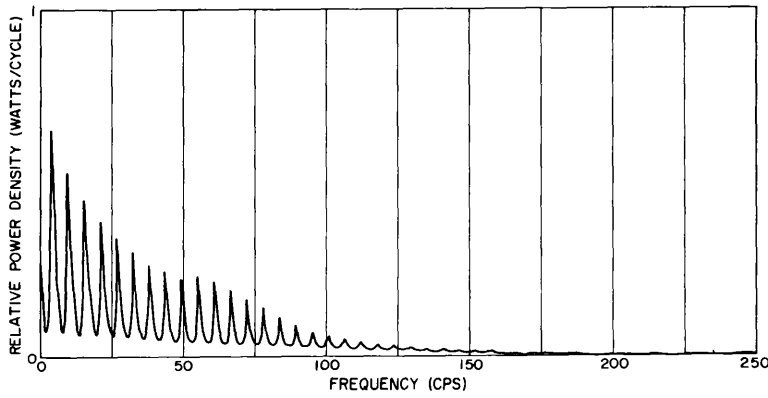


Fig. 25 - Run 4L, sea return, range 2100 yards, depression angle one degree, transmitted polarization left circular (Secret)

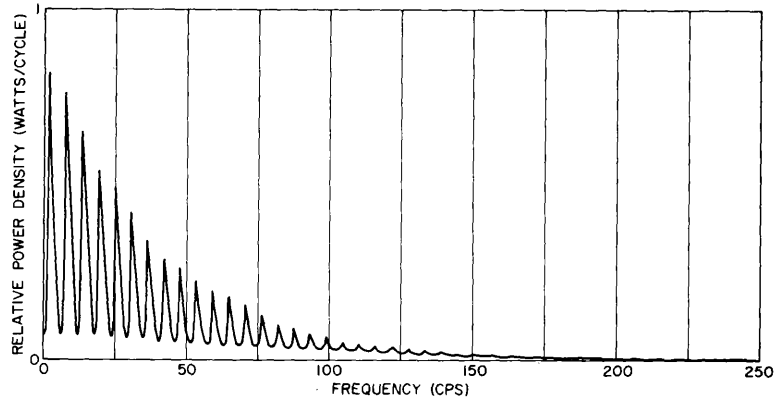


(a) Received vertical

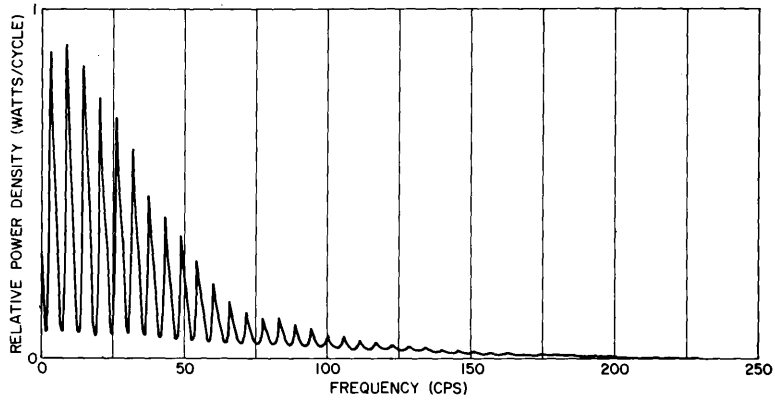


(b) Received horizontal

Fig. 26 - Run 4L, transmitted polarization left circular, two-second data sample (Secret)



(c) Received right circular



(d) Received left circular

Fig. 26 (Continued) - Run 4L, transmitted polarization left circular, two-second data sample (Secret)

Fig. 27 - Echo-amplitude distribution density for the 50 to 60 second time interval of 4L (Secret)

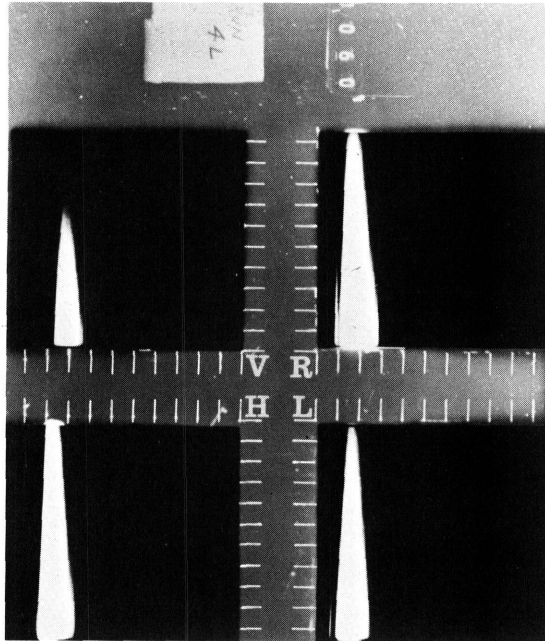


Fig. 28 - One-second sample of run 4L, displayed on high-speed oscillograph (Secret)

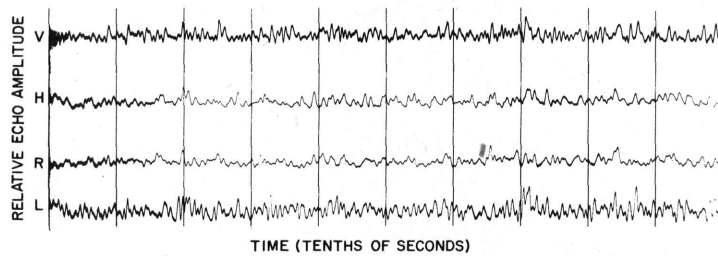
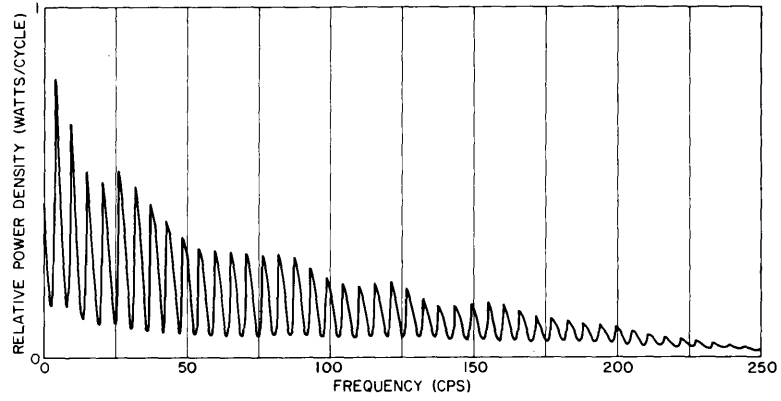
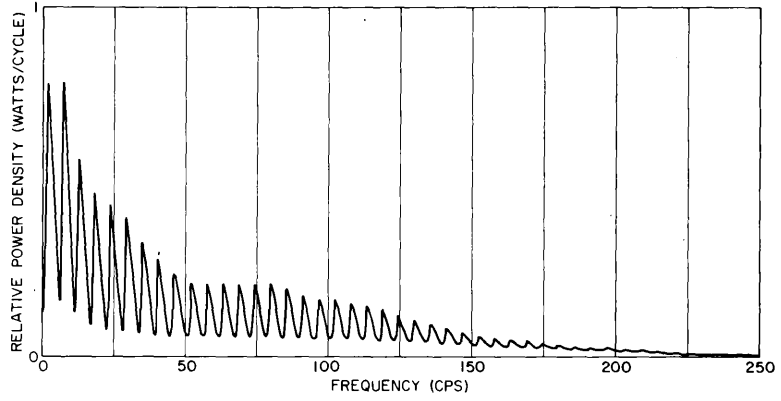


Fig. 29 - One-second sample of run 24RH (Fig. 21), displayed on high-speed oscillograph (Secret)

NAVAL RESEARCH LABORATORY

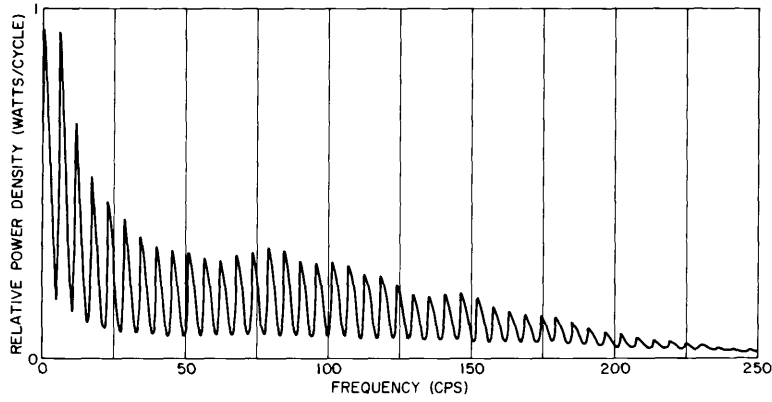


(a) Received vertical

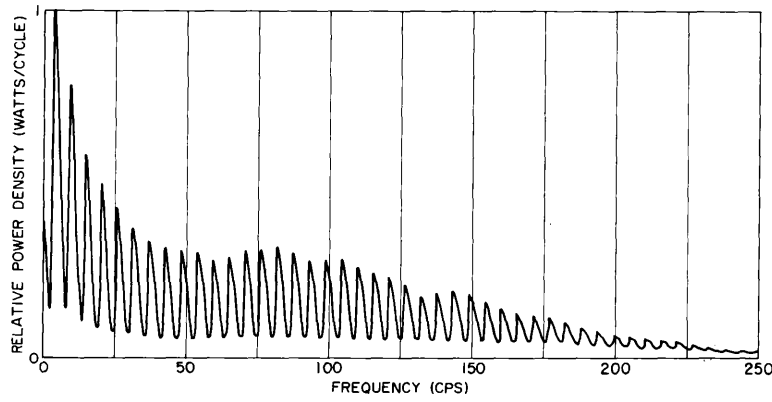


(b) Received horizontal

Fig. 30 - Run 24RH (Fig. 21), transmitted polarization right circular, time interval 19.5 to 21.5 seconds (Secret)



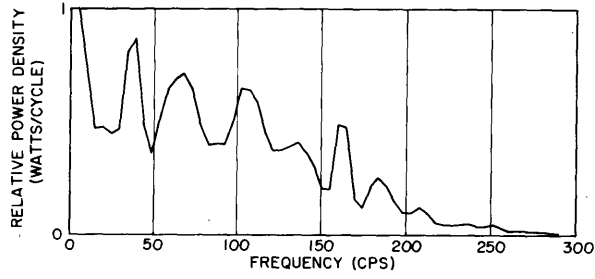
(c) Received right circular



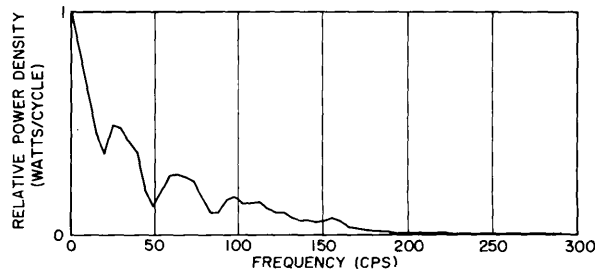
(d) Received left circular

Fig. 30 (Continued) - Run 24RH (Fig. 21), transmitted polarization right circular, time interval 19.5 to 21.5 seconds (Secret)

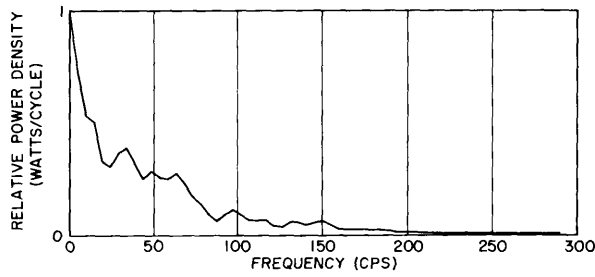
NAVAL RESEARCH LABORATORY



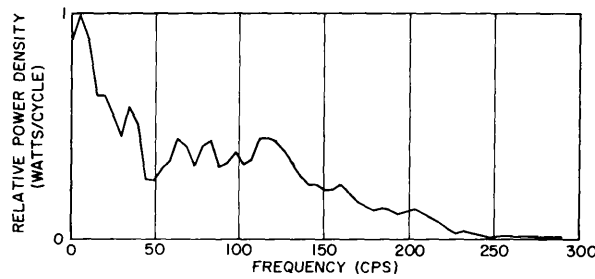
(a) Received vertical



(b) Received horizontal

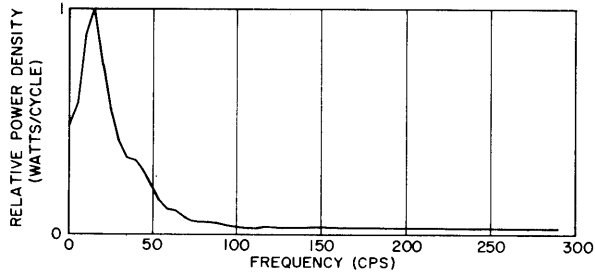


(c) Received right circular

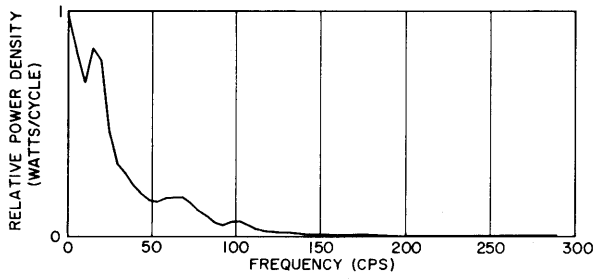


(d) Received left circular

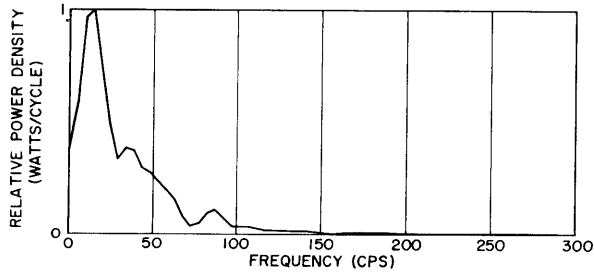
Fig. 31 - Computed power-density spectrum of the one-second chaff sample
(Secret)



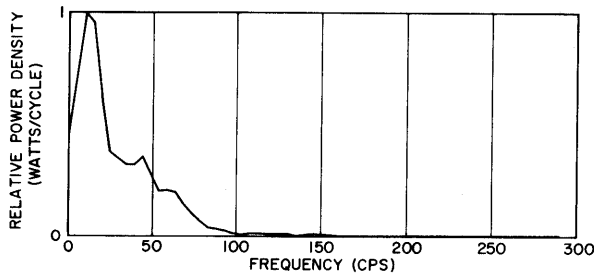
(a) Received vertical



(b) Received horizontal

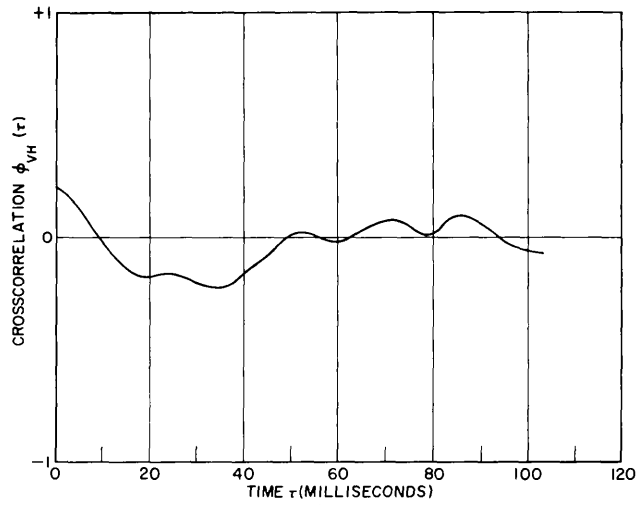


(c) Received right circular

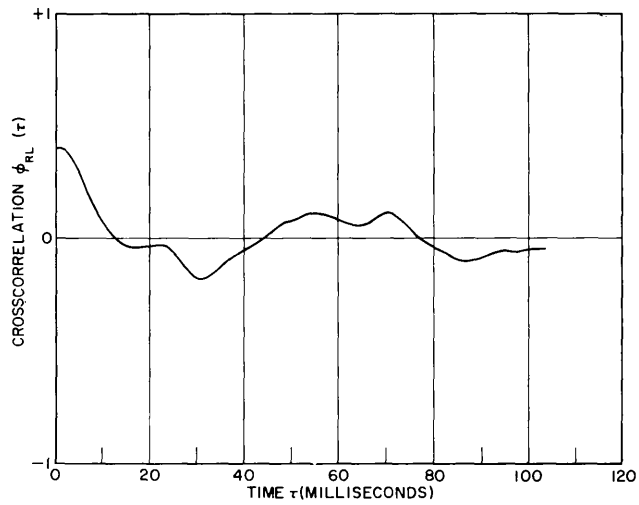


(d) Received left circular

Fig. 32 - Computed power-density spectrum of the one-second sea-return sample (Secret)

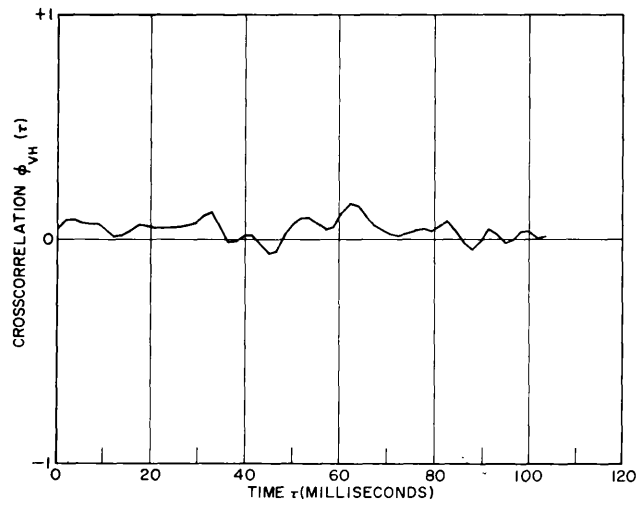


(a) Vertical and horizontal

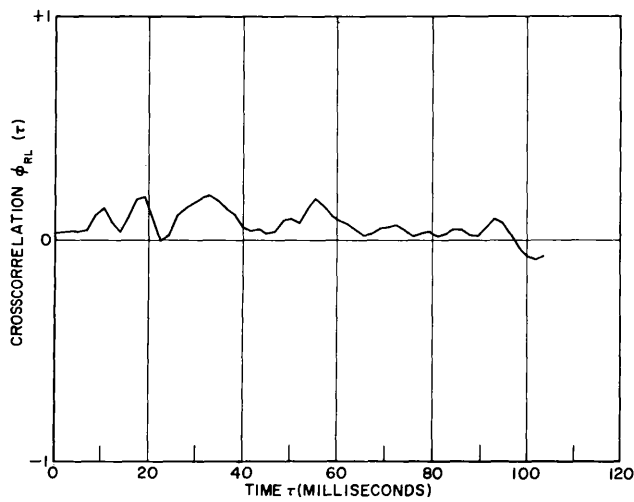


(b) Right and left circular

Fig. 33 - Crosscorrelation of components of sea return (Secret)



(a) Vertical and horizontal



(b) Right and left circular

Fig. 34 - Crosscorrelation of components of chaff (Secret)

DISTRIBUTION

DOWNGRADED AT 12-YEAR INTERVALS
 NOT AUTOMATICALLY DECLASSIFIED
 DOD DIR 5200.10

	<u>Copy No.</u>
CNO	
Attn: Code Op-03EG	1 - 2
ONR	
Attn: Code 463, Mr. C.E. Burns, Jr.	3 - 4
Code 406	5
BuWeps	
Attn: Code RRRE-2, J.F. Dibrell	6
RMWC-43, R.J. Lukes	7
RMWC-522, K.B. Pendleton	8
BuShips	
Attn: Code 670-B-1, C.L. Stec	9
USNEL, San Diego, Calif.	
Attn: Technical Library	10 - 11
USNOTS, China Lake, Calif.	
Attn: Tech. Library	12
USNPGS, Monterey, Calif.	
Attn: Tech. Library	13
USNATS, Patuxent River, Md.	
Attn: Electronics Test Div.	14
USNADC, Johnsville, Pa.	
Attn: Tech. Library	15
Aeronautical Systems Div., Wright-Patterson AFB, Dayton, Ohio	
Attn: ASD (ASAPRD-Distr.)	16
RADC, Rome, N.Y.	
Attn: RCRWE	17
AFCRC, Bedford, Mass.	
Attn: CRTOTT-2	18
OCSigO	
Attn: Ch., Research & Dev. Div.	19
USASRD, Ft. Monmouth, N.J.	
Attn: USASRD Liaison Office (3)	20 - 22
Office of the Director of Defense (R&E)	
Attn: Tech. Library Branch	23 - 24
ASTIA, Arlington, Va.	
Attn: TIPDR	25 - 34
Lincoln Laboratory, Lexington, Mass.	
Attn: Mr. G.F. Pippert	35
Lockheed Missiles & Space Div., Lockheed Aircraft Corp., Sunnyvale, Calif.	
Attn: J.R. Huynen	36

DISTRIBUTION (Cont'd)

	<u>Copy No.</u>
Sylvania Electronic Defense Laboratory, Mountain View, Calif. Attn: B.J. Lamberty	37
RCA, Moorestown, New Jersey Attn: D.L. Barton	38
General Electric, Court Street Plant, Rm. 53, Bldg. 9, Syracuse, New York Attn: L.B. Schofield	39
NRL	40 - 58